

Polar discontinuities and interfacial electronic properties of Bi₂O₂Se on SrTiO₃

Ziye Zhu,^{1,2,3} Jingshan Qi,⁴ Xiaorui Zheng,^{2,3} Xiao Lin,⁵ and Wenbin Li^{2,3,*}

¹*School of Materials Science and Engineering, Zhejiang University, Hangzhou 310027, China*

²*Key Laboratory of 3D Micro/Nano Fabrication and Characterization of Zhejiang Province, School of Engineering, Westlake University, Hangzhou 310030, China*

³*Research Center for Industries of the Future, Westlake University, Hangzhou 310030, China*

⁴*School of Science, Tianjin University of Technology, Tianjin 300384, China*

⁵*Key Laboratory for Quantum Materials of Zhejiang Province, School of Science, Westlake University, Hangzhou 310030, China*

(Dated: August 15, 2023)

The layered oxychalcogenide semiconductor Bi₂O₂Se (BOS) hosts a multitude of unusual properties including high electron mobility. Owing to similar crystal symmetry and lattice constants, the perovskite oxide SrTiO₃ (STO) has been demonstrated to be an excellent substrate for wafer-scale growth of atomically thin BOS films. However, the structural and electronic properties of the BOS/STO interface remain poorly understood. Here, through first-principles study, we reveal that polar discontinuities and interfacial contact configurations have a strong impact on the electronic properties of ideal BOS/STO interfaces. The lowest-energy [Bi-TiO₂] contact type, which features the contact between a Bi₂O₂ layer of BOS with the TiO₂-terminated surface of STO, incurs significant interfacial charge transfer from BOS to STO, producing a BOS/STO-mixed, *n*-type metallic state at the interface. By contrast, the [Se-SrO] contact type, which is the most stable contact configuration between BOS and SrO-terminated STO substrate, has a much smaller interfacial charge transfer from STO to BOS and exhibits *p*-type electronic structure with much weaker interfacial hybridization between BOS and STO. These results indicate that BOS grown on TiO₂-terminated STO substrates could be a fruitful system for exploring emergent phenomena at the interface between an oxychalcogenide and an oxide, whereas BOS grown on SrO-terminated substrates may be more advantageous for preserving the excellent intrinsic transport properties of BOS.

I. INTRODUCTION

Bismuth oxyselenide Bi₂O₂Se (BOS) has recently emerged as a layered semiconductor with a moderate bandgap ($E_g \sim 0.8$ eV), excellent air stability, ultrahigh electron mobility, and extraordinary optical sensitivity [1–4]. Room-temperature electron Hall mobility as high as $450 \text{ cm}^2\text{V}^{-1}\text{s}^{-1}$ has been measured in BOS ultrathin films (thickness ~ 6 nm) grown by chemical vapor deposition (CVD) [1]. At low temperatures, the electron mobility of such BOS thin films can reach a huge number above $20,000 \text{ cm}^2\text{V}^{-1}\text{s}^{-1}$ [1], rivalling that of two-dimensional (2D) electron gas at the LaAlO₃/SrTiO₃ (LAO/STO) interface, as well as graphene samples grown by chemical vapor deposition (CVD) [5, 6]. A huge static dielectric constant ($\epsilon_0 > 150$), which results from the proximity to a ferroelectric transition and strongly suppressing Coulombic defect scattering, is crucial for the observed ultrahigh electron mobility [7, 8]. Moreover, high-quality, stable native oxide dielectric Bi₂SeO₅ can directly form on top of BOS via layer-by-layer oxidization while preserving the high electron mobility of BOS, presenting a unique advantage of BOS over other 2D materials in terms of compatibility with existing silicon-based semiconductor technology [9].

For commercial success, functional BOS devices need to be produced at large scale and with uniform char-

acteristics. Important in this respect, it has recently been shown that high-quality, single-crystalline BOS thin films and atomic layers can be grown on STO substrates at wafer scale using CVD or molecular beam epitaxy (MBE) [10, 11], owing to the symmetry and lattice matching between BOS and STO. However, the measured electron Hall mobility of BOS thin films grown on STO substrates ($\sim 94 \text{ cm}^2\text{V}^{-1}\text{s}^{-1}$) was found to be poorer than those grown on mica substrates ($200\text{--}450 \text{ cm}^2\text{V}^{-1}\text{s}^{-1}$) [10]. Although interfacial scattering was proposed as a possible explanation of the mobility degradation, the exact microscopic origin remains unclear. Furthermore, unlike conventional layered semiconductors such as MoS₂, whose layers are bound together by van der Waals (vdW) interaction, BOS features electrostatic interaction between positively charged Bi₂O₂ layers and negatively charged Se layers. This feature could lead to stronger interfacial bonding and interaction between BOS and STO than those between a conventional vdW layered semiconductor and STO, resulting in richer interfacial phenomena. Indeed, the close symmetry and lattice-constant matching between BOS and STO, as well as between BOS and other perovskite-related materials [7], could enable the growth of a wide range of BOS-based artificial heterostructures with emergent properties. In the past, exotic phenomena such as interface superconductivity, strong electro-magnetic coupling, and fractional quantum Hall effect have been observed at the interfaces of two perovskite oxides such as between LAO and STO [12]. By contrast, little has been explored with respect to the interfacial properties be-

* liwenbin@westlake.edu.cn

tween an oxychalcogenide (to which BOS belongs) and a perovskite oxide.

These attractive prospects have motivated us to investigate the structural and electronic properties of ideal BOS/STO interfaces via first-principles calculations. The results of our study reveal that interfacial contact configurations have a strong influence on the electronic properties of the BOS/STO interfaces, which originates from the discontinuity of polarity (“polar discontinuity”) at the interface between BOS and STO. As a result of the polar discontinuity and the subsequent electronic reconstruction, the lowest-energy [Bi-TiO₂] interface, formed between a Bi₂O₂ layer of BOS and a TiO₂-terminated surface of STO, features a significant amount of interfacial charge transfer from BOS to STO, producing a *n*-type, BOS/STO-mixed metallic state at the interface. In contrast, the [Se-SrO] contact type, which is the most stable contact configuration between BOS and SrO-terminated STO substrate, belongs to *p*-type and has a much smaller interfacial charge transfer from STO to BOS, as well as much weaker interfacial electronic hybridization. These results suggest that the BOS/STO interfaces share many similarities with the LAO/STO interfaces in terms of interfacial electronic structure [5], with important implications for exploring emergent phenomena at the interfaces of oxychalcogenides and oxides, as well as for optimizing the epitaxial growth of BOS thin films on oxide substrates for practical device applications.

II. METHODS

For our calculations we adopted density functional theory (DFT) within the generalized gradient approximation (GGA) of the exchange-correlation potential, as parametrized by Perdew-Burke-Ernzerhof (PBE) [13]. The interaction between valence electrons and ionic cores was treated using projector augmented wave (PAW) potentials as implemented in the Vienna Ab initio Simulation Package (VASP) [14, 15].

To study the properties of ideal BOS/STO interface, we constructed a heterostructural model consisting of BOS and STO slabs along each of their [001] directions. The tetragonal supercell of the slab model corresponds to an in-plane repeating unit of 1×1 for both BOS and STO, and the in-plane lattice constant of the supercell follows that of STO, which simulates the coherent epitaxial growth of ultrathin BOS films on thick STO substrates [10, 11]. Regarding the specific atomistic arrangement at the interface, we considered all possible interfacial contact configurations and a series of corresponding slab models were constructed and simulated, in order to determine the lowest-energy configurations. The STO layers in the slab model is always stoichiometric. Hence, depending on the interfacial contact configurations, the surface terminations of STO slabs vary on the vacuum side. The surface of the BOS slab on the vacuum side is terminated by a layer of Se atoms passivated by hydro-

gens. The reason we use this configuration is that real BOS (001) surface usually consists of a half-full, dimerized Se layer with 50% of vacancies [2]. We find that hydrogen passivation of a full Se surface layer can effectively model the electronic properties of a BOS slab with 50% of surface Se vacancies (see **Fig. S1** in the Supplemental Materials), while circumventing the need to enlarge the in-plane unit cells of the slab, which significantly reduces the cost of computing the properties of BOS/STO interface. The chemical formulas corresponding to the slab models are (Bi₂O₂Se)₄H/(SrTiO₃)₃ and (Bi₂O₂Se)₃SeH/(SrTiO₃)₃ for interfaces with a Bi₂O₂ contact layer and Se contact layer, respectively. The slab thickness was verified to be sufficient for modelling the electronic properties of the BOS/STO interfaces (see **Fig. S2** in the Supplemental Materials).

A sufficiently large vacuum thickness of 20 Å was set in the slab model. Additional dipole correction [16] on the electrostatic potential along the vertical direction of the slab was found to have a negligible influence on the calculated properties. For the plane-wave expansion of the electronic wavefunctions, a kinetic energy cutoff of 500 eV is used. The Brillouin zone was sampled using a $9 \times 9 \times 1$ Monkhorst-Pack **k**-point mesh [17]. The convergence threshold for the self-consistency of the total energy is set to 10^{-4} eV, and all atoms in the slab were fully relaxed until the force on each atom is smaller than 0.01 eV \AA^{-1} .

III. RESULTS

A. Structure and energetics of the BOS/STO interfaces

As our goal is to understand the interfacial properties of BOS/STO, we begin with a discussion of the crystal structures of both BOS and STO. BOS has a body-centered tetragonal structure with a 4-fold symmetry (*I4/mmm* space group), with the experimental lattice parameters $a = 3.88 \text{ \AA}$, and $c = 12.16 \text{ \AA}$ [18]. The structure belongs to the *anti*-ThCr₂Si₂ type [19], and the corresponding atomistic model is illustrated in **Fig. 1(a)** (left panel). In BOS, Bi and O atoms form layered, covalently bonded frameworks with edge-sharing BiO₄ square-pyramid coordination [7, 19]. Between Bi₂O₂ layers are Se atoms arranged in a 2D square lattice. As Se is more electronegative than Bi, the Bi atoms in the Bi₂O₂ layers transfer electrons to the Se layers, resulting in positively charged [Bi₂O₂]_{*n*}^{2*n*+} layers and negatively charged [Se]_{*n*}^{2*n*-} layers, where *n* is the number of repetitive in-plane formula units. The [Bi₂O₂]_{*n*}^{2*n*+} and [Se]_{*n*}^{2*n*-} layers are bound together by forces mostly of electrostatic nature. Since the nominal charge state of Bi in BOS is +3, each Bi atom has a lone pair of $6s^2$ electrons. The lone pair electrons are stereoactive and direct in the layer-normal direction, playing a key role in stabilizing the layered structure [20].

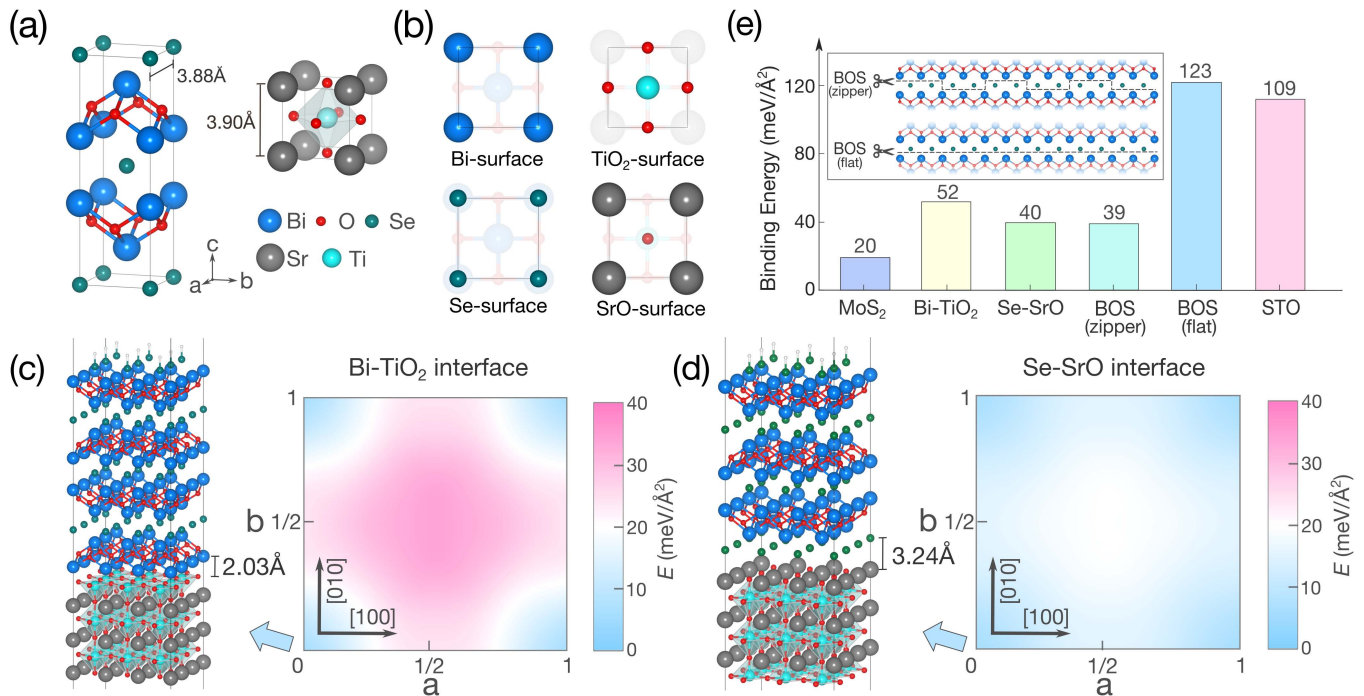


FIG. 1. (a) Atomistic models of the conventional tetragonal unit cell of $\text{Bi}_2\text{O}_2\text{Se}$ (BOS) and the cubic unit cell of SrTiO_3 (STO). (b) Illustrations of the Bi- and Se-terminated surfaces of BOS (top- and bottom-left panels), as well as the TiO_2 - and SrO-terminated surfaces of STO (top- and bottom-right panels). The representations of atoms are the same as those in (a). (c,d) DFT-relaxed atomistic structural models of the lowest-energy $[\text{Bi-TiO}_2]$ interface (c) and $[\text{Se-SrO}]$ interface (d). The distance between the Bi layer and TiO_2 layer at the $[\text{Bi-TiO}_2]$ interface is ~ 2.0 Å, whereas the distance between the Se layer and SrO layer at the $[\text{Se-SrO}]$ interface is ~ 3.2 Å. Also shown together are the corresponding changes of the interfacial binding energies with respect to the rigid relative in-plane displacements of BOS and STO slabs along the a and b axes ($[100]$ and $[010]$ directions). (e) Interlayer/interface binding energies of various systems calculated by density functional theory (DFT). The plot includes data for interlayer binding energy in MoS_2 , interface binding energies between BOS and STO that belong to the $[\text{Bi-TiO}_2]$ and $[\text{Se-SrO}]$ contact types, interlayer binding energies in BOS that correspond to zipper or flat cleavage, as well as the interlayer binding energy between the TiO_2 and SrO sheets in STO. The inset illustrates the contact breaking patterns of the zipper and flat cleavage of BOS.

The natural cleavage plane of BOS is the (001) plane. The cleavage process leaves 50 percent of Se on each of the two resulting surfaces, where most of the Se atoms left on the surfaces have a dimerized structure [2]. The interlayer binding energy corresponding to this dimerized “zipper” cleavage mode [21] has a small value of ~ 39 $\text{meV}/\text{\AA}^2$, as obtained from our DFT calculations. By contrast, the DFT-calculated binding energy between atomically flat Bi_2O_2 and Se layers, which corresponds to all the Se atoms on one side of the two surfaces created by cleavage, has a much higher value of ~ 123 $\text{meV}/\text{\AA}^2$. To put these numbers in perspective, the interlayer binding energy of MoS_2 is merely ~ 20 $\text{meV}/\text{\AA}^2$ [22]. The distinct bonding characteristics of BOS suggest that its interfacial properties could be rather different from those of conventional layered semiconductors.

On the other hand, STO has a typical cubic perovskite structure with $Pm\bar{3}m$ space group and a lattice constant of 3.90 Å [23], which is also illustrated in the right panel of Fig. 1(a). In the $[001]$ direction, STO has alternate stacking of planar TiO_2 and SrO atomic sheets. Thus,

the (001) surface of STO has two distinct terminations, either TiO_2 - or SrO-terminated. As the nominal charge of Sr, Ti, and O in STO are +2, +4, and -2 , respectively, in the simple ionic limit, each TiO_2 or SrO sheet can be considered charge neutral [12]. Normally, the surface of STO substrates obtained by cleavage or cutting consists of an equal amount of TiO_2 - and SrO-terminated domains separated by half-unit-cell steps [24]. However, simple chemical treatment methods have been developed to achieve fully TiO_2 -terminated surfaces [25–27]. The opposite single-terminated SrO surfaces can be obtained either by annealing STO substrates in air at high temperatures [28], or by depositing a SrO monolayer on top of a single-terminated TiO_2 surface [12, 29].

The (001) planes of BOS and STO are symmetry matched (both have 2D square lattices), with a small lattice-constant difference of 0.5% (3.88 Å versus 3.90 Å). Therefore, when a BOS thin film is grown on the (001) surface of a STO substrate, coherent interface can form, wherein the in-plane lattice constants of BOS follow those of STO [10, 11]. Since the (001) surface of STO can

be TiO₂- or SrO-terminated, whereas that of BOS can be terminated with a Bi₂O₂ or Se layer, as illustrated in **Fig. 1(b)**, four atomically sharp interfacial contact types are theoretically possible between BOS and STO. The [Bi-TiO₂] contact type involves the direct contact of a Bi₂O₂ layer of BOS on top of a TiO₂-terminated STO. This contact type has been experimentally observed in BOS thin films grown on STO by both CVD and molecular beam epitaxy [10, 11]. The [Se-SrO] contact type corresponds to a Se layer of BOS on SrO-terminated STO. The [Se-TiO₂] and [Bi-SrO] contact types have similar connotations.

In each of the four contact types, additional in-plane translational degrees of freedom exist. We have considered all the possible high-symmetry, coherent interfacial contact configurations between the (001) surfaces of BOS and STO, and carried out DFT calculations of the corresponding interfacial binding energies. Here, the interfacial binding energy is defined as the energy needed to separate an interface. The results of our calculations indicate that the [Bi-TiO₂] contact type, in its most stable configuration, has the highest binding energy of 52 meV/Å² among all four interfacial contact types. The binding energy of the [Se-SrO] interface has a close value of 40 meV/Å². In contrast, the other two interfacial contact types, namely [Se-TiO₂] and [Bi-SrO], have much smaller binding energies of 16 meV/Å² and 5 meV/Å², respectively. Hence, when BOS is grown on a TiO₂-terminated STO substrate, the equilibrium interfacial contact type should be [Bi-TiO₂], which is in consistent with previous experimental observations [10, 11]. On the other hand, if the STO substrate is SrO-terminated, the [Se-SrO] contact type should be energetically much more competitive than the [Bi-SrO] type. The energetic order between different contact types can be understood in terms of their interfacial charge transfer properties, which will be discussed latter.

The lowest-energy in-plane alignments between BOS and STO in the [Bi-TiO₂] and [Se-SrO] contact types are in accordance with the illustrated Bi- and Se-surfaces of BOS, as well as the TiO₂- and SrO-surfaces of STO in **Fig. 1(b)**. Specifically, in the [Bi-TiO₂] contact type, the Bi atoms of BOS sit above the four-fold hollow sites of O atoms and align with the Sr atoms below, in agreement with experimental observations [10, 11]. On the other hand, in the [Se-SrO] contact type, Se atoms are located directly on top of Sr atoms. Additional side views of the [Bi-TiO₂] and [Se-SrO] contact types are shown in **Fig. 1(c,d)** and Supplementary **Fig. S3**.

In **Fig. 1(e)** we compare the binding energies of [Bi-TiO₂] and [Se-SrO] interfaces with the interfacial or interlayer binding energies in other systems, including the vdW interlayer binding energy of MoS₂, the interlayer binding energy of BOS that corresponds to zipper or atomically flat cleavage, as well as the binding energy between TiO₂ and SrO sheets in STO. It is noted that in the flat cleavage mode of BOS, which leaves all Se atoms on one side of the cleaved surface, the corre-

sponding binding energy (123 meV/Å²) is even larger than that of between TiO₂ and SrO sheets in STO (109 meV/Å²). This shows that the interlayer electrostatic interaction between [Bi₂O₂]_n²ⁿ⁺ and [Se]_n²ⁿ⁻ layers in BOS is by no means weak. Furthermore, the binding energies of the [Bi-TiO₂] and [Se-SrO] interfaces are both several times higher than that between MoS₂ layers. The relatively strong interfacial binding between BOS and STO, in combination with symmetry and close lattice-constant matching, makes coherent epitaxial growth of BOS on STO and other perovskite-related materials growth possible [10, 11]. This creates an exciting opportunity to generate a large variety of novel heterostructures between the oxychalcogenide BOS and perovskite oxides.

B. Electronic properties of the ideal BOS/STO interfaces

Having studied the contact configurations and energetics of the BOS/STO interfaces, we next investigate their electronic properties. **Fig. 2(a,b)** show the DFT-computed electronic band structures of the heterostructural slab models of the [Bi-TiO₂] and [Se-SrO] interfaces, which correspond to the atomistic structural models in **Fig. 1(d)** and **1(e)**, respectively. In the case of the [Bi-TiO₂] interface, the Fermi level (E_F) is located above the CBM and crosses both the BOS and STO components, resulting in a *n*-type metallic phase. Notably, there is a distinct hybridization of electronic states between BOS and STO near the E_F along the M- Γ and X-M directions in its 2D Brillouin zone. On the other hand, for the [Se-SrO] contact interface, the E_F shifts to the valence band, resulting in a *p*-type metallic state. However, no noticeable hybridization between BOS and STO can be observed from the projected band structure in this contact type.

To probe the origin of the metallic states, we compute the electronic band structures of isolated slabs of BOS and STO. **Fig. S4** shows that the Fermi levels of STO slabs are always located in the band gap regardless of the surface termination, corresponding to an insulating state. In contrast, in a Bi₂O₂-terminated BOS slab, the Fermi levels move into the conduction band, while in a Se-terminated slab, the Fermi level is in the valence band. When a BOS slab and a STO slab are put into contact, charge transfer can occur between BOS and STO slabs in order to reach a uniform electron chemical potential across the interface. In the case of [Bi-TiO₂] interface, after electronic reconstruction, the Fermi level crosses the conduction bands of both BOS and STO, indicating charge transfer from the BOS slab to the STO slab, while in the case of [Se-SrO] interface, the Fermi level crosses the valence bands of both BOS and STO, indicating a reverse direction of charge transfer from STO to BOS.

The different charge transfer behavior is confirmed by explicitly computing the amount of interfacial charge

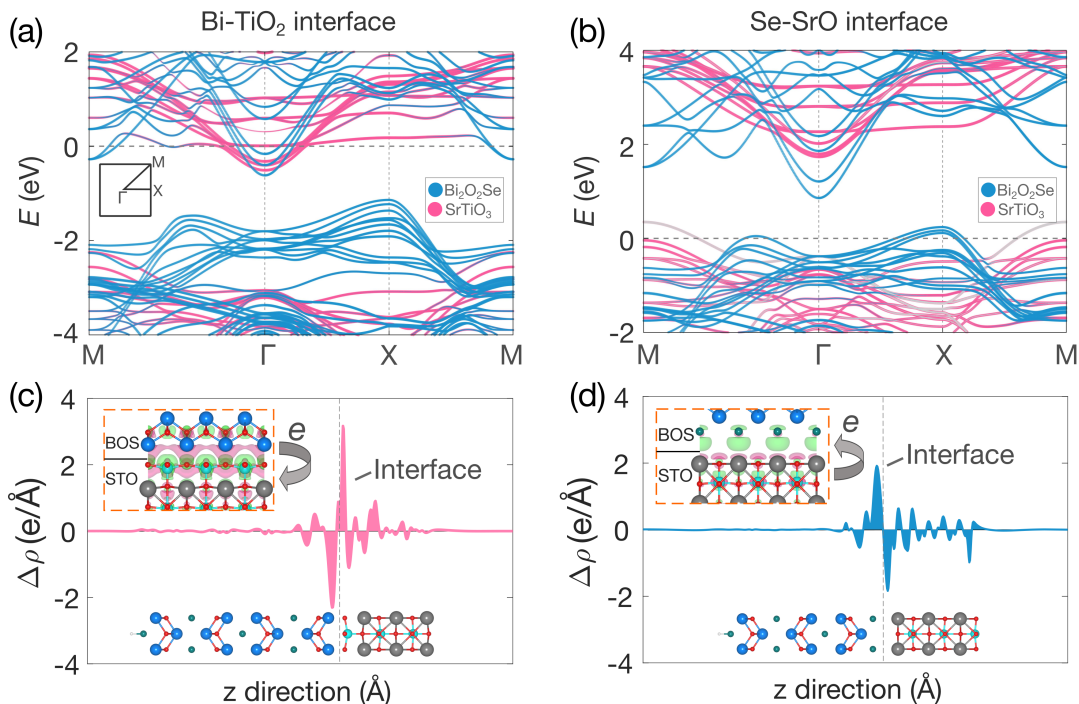


FIG. 2. **(a,b)** Density functional theory (DFT) calculated electronic band structures of ideal BOS/STO interface with [Bi-TiO₂] and [Se-SrO] contact types. The inset in **(a)** is the corresponding reciprocal space path. The Fermi level is set to energy zero. The gray lines in **(b)** denote that the corresponding electronic states derive from the surface states of the STO slab on the opposite side of the interface. **(c,d)** Planar averaged electron density differences of the [Bi-TiO₂] **(c)** and [Se-SrO] **(d)** contact types with respect to isolated slabs, which are calculated as $\Delta\rho = \rho_{\text{BOS/STO}} - \rho_{\text{BOS}} - \rho_{\text{STO}}$. The inset figures in dashed boxes are plots of charge density differences, drawn using the VESTA software [30]. The green (pink) color corresponds to charge accumulation (depletion) and the isosurfaces correspond to $\Delta\rho$ equal to $0.0015 \text{ e}/\text{\AA}^3$.

transfer at the two types of BOS/STO interfaces. As shown in **Fig. 2(c,d)**, charge accumulation and depletion on the side of STO are found in the [Bi-TiO₂] and [Se-SrO] contact types, respectively. In addition to the opposite charge transfer direction, the magnitude of charge transfer is significantly different between the two. Bader charge analysis [31] reveals that about 0.5 electron per 2D unit cell ($e/u.c$) is transferred from BOS to STO in the [Bi-TiO₂] contact type, whereas the corresponding number is 0.2 $e/u.c$ from STO to BOS in the [Se-SrO] contact type. The stronger interfacial charge transfer and electronic hybridization observed at the [Bi-TiO₂] contact interface explain its higher interfacial binding energy than the [Se-SrO] contact type, as discussed in the previous section.

IV. DISCUSSIONS

The intriguing electronic properties of the BOS/STO interfaces originate from polar discontinuity at the contact interfaces. Unlike vdW layered materials such as MoS₂, BOS consists of alternate stacking of the charged [Bi₂O₂]²⁺ and [Se]²⁻ layers along the [001] direction. Each Bi₂O₂ layer donates two electrons per 2D unit cell

to the neighboring Se layers, resulting in interlayer electrostatic interaction between the [Bi₂O₂]²⁺ and [Se]²⁻ layers. Here, the nominal charge of Bi, O, and Se are 3+, 2-, and 2- in the simple ionic limit, respectively. In comparison, STO has alternate stacking of charge neutral TiO₂ and SrO layers along the [001] direction, with the nominal charges of Ti, Sr, O being 4+, 2+, and 2- in the simple ionic limit, respectively. Hence, along the [001] direction, BOS is polar while STO is not, and as a result, there is a polar discontinuity at the interface between BOS and STO, similar to that at the LAO/STO interface [5, 12, 32]. For the [Bi-TiO₂] contact type of the BOS/STO interface, the polar discontinuity can be denoted as (Bi₂O₂)²⁺/(TiO₂)⁰, while for the [Se-SrO] contact type, it can be denoted as (Se)²⁻/(SrO)⁰.

In the absence of interfacial electronic or atomic reconstruction, polar discontinuity at heterostructural interface can lead to “polar catastrophe”, where the electrostatic potential generated by the charged layers grows quickly away from the interface and diverges in the bulk limit [32–34]. In heterostructures formed by growing a conventional polar semiconductor on a non-polar semiconductor, such as GaAs on Si, such potential divergence is avoided via atomic reconstruction at the interface through atomic disordering or a change in stoichiom-

etry [35–37]. However, in oxide heterostructures where certain ions can assume multiple valencies, such as Ti in STO, whose valence can change from Ti^{4+} to Ti^{3+} , polar catastrophe can be avoided via electronic reconstruction, specifically through interfacial charge transfer that leads to mixed valencies of certain ions [32–34]. Such interfacial electronic construction was considered to be responsible for the observation of 2D electron gas at the $(\text{LaO})^+ / (\text{TiO}_2)^0$ interface between LAO and STO [5].

The interfacial electronic properties of the BOS/STO interfaces thus share significant similarities with the LAO/STO interfaces. The polar discontinuity of the $[\text{Bi-TiO}_2]$ contact interface, explicitly written as $(\text{Bi}_2\text{O}_2)^{2+} / (\text{TiO}_2)^0$, corresponds to that of the $(\text{LaO})^+ / (\text{TiO}_2)^0$ interface between LAO and STO. After electronic reconstruction in self-consistent DFT calculations, this interface type involves charge transfer from the Bi_2O_2 layer to the TiO_2 layer in the amount of $\sim 0.5 e/\text{u.c.}$, as illustrated in **Fig. 3(a)**. Conceptually, one can also start from the atomic limit and then allow ionization of the elements. In bulk BOS, a Bi_2O_2 layer donates $2 e/\text{u.c.}$ of electrons to its two neighboring Se layers. However, for the Bi_2O_2 layer at the $\text{Bi}_2\text{O}_2/\text{TiO}_2$ interface, only one Se layer on one side of the interface is available to accept electrons. Hence, the Bi_2O_2 layer at the interface have excess electrons on the order of $1 e/\text{u.c.}$, which leads to a *n*-type interface. These excess electrons can be partially transferred to the TiO_2 layer on the other side of the interface, in the process partially changing the Ti valency from Ti^{4+} to Ti^{3+} .

On the other hand, the polar discontinuity at the $[\text{Se-SrO}]$ contact interface, written as $(\text{Se})^{2-} / (\text{SrO})^0$, is akin to the $(\text{AlO}_2)^- / (\text{SrO})^0$ interface between LAO and STO. In this case, the Se layer at the interface only has one neighboring Bi_2O_2 layer from which it can receive electrons, leading to a *p*-type electronic state. This electron deficiency could be mitigated by charge transfer from the SrO layer on the STO side of the interface. However, since it is energetically costly to induce mixed valency for either Sr or O, the amount of charge transfer from the SrO layer is rather limited. In our DFT calculation of the ideal $[\text{Se-SrO}]$ interface, the amount of charge transfer is calculated to be $\sim 0.2 e/\text{u.c.}$, as illustrated in **Fig. 3(b)**. In fact, we find that the transferred charge in our DFT calculation mainly originates from the surface state of the STO slab on the opposite side of the contact interface. Given that in real experiments, the SrO-terminated substrate is rather thick, charge transfer from the STO side to the BOS side would be further hampered. Since electronic reconstruction at the $[\text{Se-SrO}]$ contact interface is energetically unfavorable, atomic reconstruction is expected to occur in this contact type in real systems, where the generation of Se vacancies or O vacancies near the interface can provide the extra electrons that compensate the *p*-type carriers. Indeed, in the *p*-type $(\text{AlO}_2)^- / (\text{SrO})^0$ interface between LAO and STO, oxygen vacancies play a central role in avoiding polar catastrophe and lead to an insulating interface instead

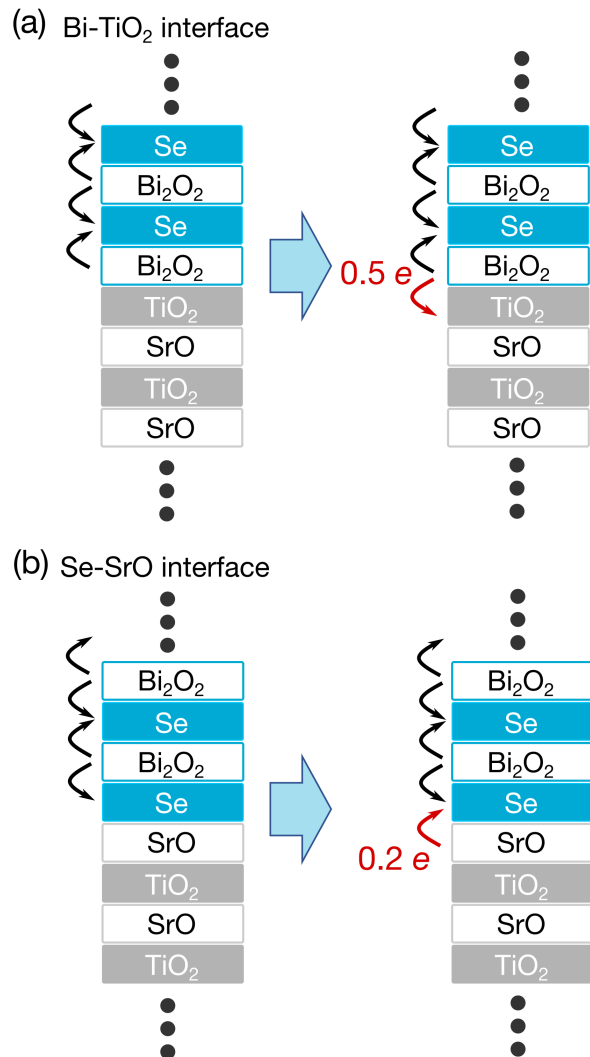


FIG. 3. Schematic diagrams of polar discontinuities and charge transfer at the interfaces between BOS and STO. (a) The $[\text{Bi-TiO}_2]$ contact interface. (b) The $[\text{Se-SrO}]$ contact interface.

of *p*-type hole transport [5, 33]. Similar phenomena could happen at the $[\text{Se-SrO}]$ contact type of the BOS/STO interface.

It is worth emphasizing that the polar discontinuities of the BOS/STO interfaces arise from the charged layered structure of BOS with interlayer electrostatic interaction, which is absent in heterostructures of typical vdW layered materials such as MoS_2 grown on STO. Consequently, the substrate used for growing BOS thin films could have a significant influence on their experimentally measured electronic properties. When mica substrates are used for the CVD growth of BOS [1], the interfacial structure involves the surface K^+ layer of mica in contact with the Se layer of BOS, as illustrated in **Fig. 4(a)**, which has been experimentally observed using atomic-scale scanning transmission electron microscopy (STEM) [38]. Since the K^+ layer of mica is electronically

inert, charge transfer between BOS and mica shall be minimal. By contrast, for BOS thin films grown on TiO_2 -terminated STO substrates, the interface belongs to the $[\text{Bi-TiO}_2]$ contact type [10, 11], as schematically depicted in **Fig. 4(b)**. As we have discussed above, due to polar discontinuity and the ability of Ti^{4+} to undergo valence change, significant interfacial charge transfer from BOS to STO is expected to occur. Consequently, the electronic states responsible for the n -type electron transport have contributions from both BOS and STO. As the electron effective mass of STO is larger than that of BOS (see also Fig. 2(a)), the resulting measured room-temperature electron mobility of BOS grown on TiO_2 -terminated STO substrates shall be smaller than those measured from BOS samples grown on mica substrates, which was indeed found in experiments [10]. Nonetheless, the strong interfacial interaction means that novel electronic or magnetic properties could emerge from the $[\text{Bi-TiO}_2]$ contact type of the BOS/STO interface, as in the case of LAO grown on TiO_2 -terminated STO substrates [12].

For the $[\text{Se-SrO}]$ contact configuration, the interfacial charge transfer is much weaker, resulting in a weakly p -type electronic structure and energetically well-separated conduction bands of BOS and STO (Fig. 2(b)). Although the formation of Se vacancies and possibly oxygen vacancies, promoted by the polar discontinuity at the interface, are likely to compensate the hole carriers, the p -type behavior before reconstruction suggests that field-effect transistors fabricated from BOS layers grown on SrO-terminated STO substrate, as illustrated in **Fig. 4(c)**, may circumvent the problem of high residual electron carrier concentrations that has plagued BOS-based transistor devices [39], and may even pave the way for realizing p -type transistors based on BOS.

V. CONCLUSIONS

In conclusion, we have performed systematic first-principles investigations of the energetic and electronic properties of ideal BOS/STO interfaces, revealing the crucial effect of interfacial contact type and polar discontinuity on the interfacial properties. For BOS grown on TiO_2 -terminated STO, a Bi_2O_2 layer in contact with a surface TiO_2 layer of STO, denoted by $[\text{Bi-TiO}_2]$, is found to be the lowest-energy interface configuration, in consistent with experimental observations. Due to the polar discontinuity between BOS and STO and the ability of titanium ions to exist in mixed valencies, a significant charge transfer from BOS to STO occurs in the $[\text{Bi-TiO}_2]$ contact type. This leads to a n -type interface with a mixed metallic state of BOS and STO, which is likely responsible for the lower electron mobility observed in BOS grown on TiO_2 -terminated STO substrates as compared to BOS grown on electrically more inert substrates such as mica. For SrO-terminated STO substrates, we find that the lowest-energy contact configuration between

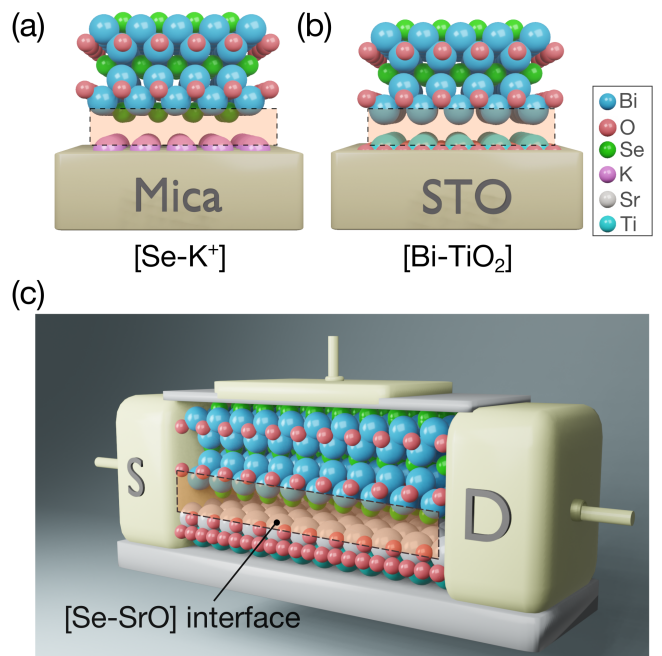


FIG. 4. (a,b) Illustration of the contact interface of BOS thin films grown on a mica and TiO_2 -terminated STO substrates. (c) Schematic illustration of a field-effect transistor (FET) device directly fabricated on a BOS layer grown on a SrO-terminated STO substrate, with the $[\text{Se-SrO}]$ contact interface indicated by orange shade.

BOS and STO is a Se layer on a SrO layer, denoted by $[\text{Se-SrO}]$. This contact configuration has a much weaker interfacial charge transfer, resulting in a p -type electronic structure. The asymmetry in interfacial charge transfer properties between $[\text{Bi-TiO}_2]$ and $[\text{Se-SrO}]$ interfaces can be explained in terms of the ability of Ti^{4+} to undergo a change in valence to Ti^{3+} in a TiO_2 layer, whereas such a change in valence is energetically costly for Sr^{2+} or O^{2-} in a SrO layer. In real experiments, the hole carriers at the $[\text{Se-SrO}]$ interface may be compensated by ionized Se or oxygen vacancies. However, the energetically well-separated conduction bands of BOS and STO in this contact type suggests that the excellent electron transport properties of BOS may be better preserved in this contact type. These results indicate that BOS grown on TiO_2 -terminated STO substrates could be a fruitful system for exploring emergent interface phenomena between an oxychalcogenide and an oxide, whereas SrO-terminated STO substrates may be desirable for wafer-scale growth of BOS films with excellent carrier transport properties.

ACKNOWLEDGMENTS

This work is supported by NSFC under Project No. 62004172. W.L. also acknowledges the support by Research Center for Industries of the Future at Westlake University under Award No. WU2022C041. X.L. and

X.Z. thank the Westlake Multidisciplinary Research Initiative Center (MRIC) under Grant No. MRIC20200402. The authors thank Shu Zhao and Xiaoping Yao for help-

ful discussions, as well as the High-Performance Computing Center of Westlake University for technical assistance.

-
- [1] J. Wu, H. Yuan, M. Meng, C. Chen, Y. Sun, Z. Chen, W. Dang, C. Tan, Y. Liu, J. Yin, Y. Zhou, S. Huang, H. Q. Xu, Y. Cui, H. Y. Hwang, Z. Liu, Y. Chen, B. Yan, and H. Peng, High electron mobility and quantum oscillations in non-encapsulated ultrathin semiconducting $\text{Bi}_2\text{O}_2\text{Se}$, *Nat. Nanotechnology* **12**, 530 (2017).
- [2] C. Chen, M. Wang, J. Wu, H. Fu, H. Yang, Z. Tian, T. Tu, H. Peng, Y. Sun, X. Xu, J. Jiang, N. B. M. Schröter, Y. Li, D. Pei, S. Liu, S. A. Ekahana, H. Yuan, J. Xue, G. Li, J. Jia, Z. Liu, B. Yan, H. Peng, and Y. Chen, Electronic structures and unusually robust bandgap in an ultrahigh-mobility layered oxide semiconductor, $\text{Bi}_2\text{O}_2\text{Se}$, *Sci. Adv.* **4**, eaat8355 (2018).
- [3] J. Yin, Z. Tan, H. Hong, J. Wu, H. Yuan, Y. Liu, C. Chen, C. Tan, F. Yao, T. Li, Y. Chen, Z. Liu, K. Liu, and H. Peng, Ultrafast and highly sensitive infrared photodetectors based on two-dimensional oxyselenide crystals, *Nat. Commun.* **9**, 3311 (2018).
- [4] T. Li and H. Peng, 2D $\text{Bi}_2\text{O}_2\text{Se}$: an emerging material platform for the next-generation electronic industry, *Acc. Mater. Res.* **2**, 842 (2021).
- [5] A. Ohtomo and H. Y. Hwang, A high-mobility electron gas at the $\text{LaAlO}_3/\text{SrTiO}_3$ heterointerface, *Nature* **427**, 423 (2004).
- [6] N. Petrone, C. R. Dean, I. Meric, A. M. van der Zande, P. Y. Huang, L. Wang, D. Muller, K. L. Shepard, and J. Hone, Chemical vapor deposition-derived graphene with electrical performance of exfoliated graphene, *Nano Lett.* **12**, 2751 (2012).
- [7] Z. Zhu, X. Yao, S. Zhao, X. Lin, and W. Li, Giant modulation of the electron mobility in semiconductor $\text{Bi}_2\text{O}_2\text{Se}$ via incipient ferroelectric phase transition, *J. Am. Chem. Soc.* **144**, 4541 (2022).
- [8] Z. Xu, J. Wang, T. Wang, W. Hu, X. Yang, and X. Lin, Huge permittivity and premature metallicity in $\text{Bi}_2\text{O}_2\text{Se}$ single crystals, *Sci. China Phys. Mech.* **64**, 267312 (2021).
- [9] T. Li, T. Tu, Y. Sun, H. Fu, J. Yu, L. Xing, Z. Wang, H. Wang, R. Jia, J. Wu, C. Tan, Y. Liang, Y. Zhang, C. Zhang, Y. Dai, C. Qiu, M. Li, R. Huang, L. Jiao, K. Lai, B. Yan, P. Gao, and H. Peng, A native oxide high- κ gate dielectric for two-dimensional electronics, *Nat. Electron.* **3**, 473 (2020).
- [10] C. Tan, M. Tang, J. Wu, Y. Liu, T. Li, Y. Liang, B. Deng, Z. Tan, T. Tu, Y. Zhang, C. Liu, J.-H. Chen, Y. Wang, and H. Peng, Wafer-scale growth of single-crystal 2D semiconductor on perovskite oxides for high-performance transistors, *Nano Lett.* **19**, 2148 (2019).
- [11] Y. Liang, Y. Chen, Y. Sun, S. Xu, J. Wu, C. Tan, X. Xu, H. Yuan, L. Yang, Y. Chen, P. Gao, J. Guo, and H. Peng, Molecular beam epitaxy and electronic structure of atomically thin oxyselenide films, *Adv. Mater.* **31**, 1901964 (2019).
- [12] H. Y. Hwang, Y. Iwasa, M. Kawasaki, B. Keimer, N. Nagaosa, and Y. Tokura, Emergent phenomena at oxide interfaces, *Nat. Mater.* **11**, 103 (2012).
- [13] J. P. Perdew, K. Burke, and M. Ernzerhof, Generalized gradient approximation made simple, *Phys. Rev. Lett.* **77**, 3865 (1996).
- [14] P. E. Blöchl, Projector augmented-wave method, *Phys. Rev. B* **50**, 17953 (1994).
- [15] G. Kresse and J. Furthmüller, Efficient iterative schemes for ab initio total-energy calculations using a plane-wave basis set, *Phys. Rev. B* **54**, 11169 (1996).
- [16] L. Bengtsson, Dipole correction for surface supercell calculations, *Phys. Rev. B* **59**, 12301 (1999).
- [17] H. J. Monkhorst and J. D. Pack, Special points for brillouin-zone integrations, *Phys. Rev. B* **13**, 5188 (1976).
- [18] H. Boller, Die kristallstruktur von $\text{Bi}_2\text{O}_2\text{Se}$, *Monatshefte für Chemie* **104**, 916 (1973).
- [19] R. Hoffmann and C. Zheng, Making and breaking bonds in the solid state: the ThCr_2Si_2 structure, *J. Phys. Chem.* **89**, 4175 (1985).
- [20] A. L. J. Pereira, D. Santamaría-Pérez, J. Ruiz-Fuertes, F. J. Manjón, V. P. Cuenca-Gotor, R. Vilaplana, O. Gomis, C. Popescu, A. Muñoz, P. Rodríguez-Hernández, A. Segura, L. Gracia, A. Beltrán, P. Ruleova, C. Drasar, and J. A. Sans, Experimental and theoretical study of $\text{Bi}_2\text{O}_2\text{Se}$ under compression, *J. Phys. Chem. C* **122**, 8853 (2018).
- [21] Q. Wei, R. Li, C. Lin, A. Han, A. Nie, Y. Li, L.-J. Li, Y. Cheng, and W. Huang, Quasi-two-dimensional Se-terminated bismuth oxychalcogenide ($\text{Bi}_2\text{O}_2\text{Se}$), *ACS Nano* **13**, 13439 (2019).
- [22] T. Björkman, A. Gulans, A. V. Krasheninnikov, and R. M. Nieminen, Are we van der Waals ready?, *J. Phys.: Condens. Matter* **24**, 424218 (2012).
- [23] Y. A. Abramov, V. G. Tsirelson, V. E. Zavodnik, S. A. Ivanov, and I. D. Brown, The chemical bond and atomic displacements in SrTiO_3 from X-ray diffraction analysis, *Acta. Cryst. B* **51**, 942 (1995).
- [24] M. Huijben, A. Brinkman, G. Koster, G. Rijnders, H. Hilgenkamp, and D. H. A. Blank, Structure-property relation of SrTiO_3 interfaces, *Adv. Mater.* **21**, 1665 (2009).
- [25] M. Kawasaki, K. Takahashi, T. Maeda, R. Tsuchiya, M. Shinohara, O. Ishiyama, T. Yonezawa, M. Yoshimoto, and H. Koinuma, Atomic control of the SrTiO_3 crystal surface, *Science* **266**, 1540 (1994).
- [26] G. Koster, B. L. Kropman, G. J. H. M. Rijnders, D. H. A. Blank, and H. Rogalla, Quasi-ideal strontium titanate crystal surfaces through formation of strontium hydroxide, *Appl. Phys. Lett.* **73**, 2920 (1998).
- [27] T. Ohnishi, K. Shibuya, M. Lippmaa, D. Kobayashi, H. Kumigashira, M. Oshima, and H. Koinuma, Preparation of thermally stable TiO_2 -terminated SrTiO_3 (100) substrate surfaces, *Appl. Phys. Lett.* **85**, 272 (2004).
- [28] R. Bachelet, F. Sánchez, F. J. Palomares, C. Ocal, and J. Fontcuberta, Atomically flat SrO-terminated SrTiO_3 (001) substrate, *Appl. Phys. Lett.* **95**, 141915 (2009).
- [29] M. Radovic, N. Lampis, F. M. Granozio, P. Perna, Z. Ristic, M. Salluzzo, C. M. Schlepütz, and U. S. di Uccio,

- Growth and characterization of stable SrO-terminated SrTiO₃ surfaces, *Appl. Phys. Lett.* **94**, 022901 (2009).
- [30] K. Momma and F. Izumi, Vesta 3 for three-dimensional visualization of crystal, volumetric and morphology data, *J. Appl. Crystallogr.* **44**, 1272 (2011).
- [31] G. Henkelman, A. Arnaldsson, and H. Jónsson, A fast and robust algorithm for bader decomposition of charge density, *Comput. Mater. Sci.* **36**, 354 (2006).
- [32] J. Mannhart, D. Blank, H. Hwang, A. Millis, and J.-M. Triscone, Two-dimensional electron gases at oxide interfaces, *MRS Bull.* **33**, 1027 (2008).
- [33] N. Nakagawa, H. Y. Hwang, and D. A. Muller, Why some interfaces cannot be sharp, *Nat. Mater.* **5**, 204 (2006).
- [34] H. Y. Hwang, Tuning interface states, *Science* **313**, 1895 (2006).
- [35] G. A. Baraff, J. A. Appelbaum, and D. R. Hamann, Self-consistent calculation of the electronic structure at an abrupt GaAs-Ge interface, *Phys. Rev. Lett.* **38**, 237 (1977).
- [36] W. A. Harrison, E. A. Kraut, J. R. Waldrop, and R. W. Grant, Polar heterojunction interfaces, *Phys. Rev. B* **18**, 4402 (1978).
- [37] H. Kroemer, Polar-on-nonpolar epitaxy, *J. Cryst. Growth* **81**, 193 (1987).
- [38] C. Hong, Y. Tao, A. Nie, M. Zhang, N. Wang, R. Li, J. Huang, Y. Huang, X. Ren, Y. Cheng, and X. Liu, Inclined ultrathin Bi₂O₂Se films: a building block for functional van der waals heterostructures, *ACS Nano* **14**, 16803 (2020).
- [39] T. Wang, Z. Xu, Z. Zhu, M. Wu, Z. Lou, J. Wang, W. Hu, X. Yang, T. Sun, X. Zheng, W. Li, and X. Lin, Highly insulating phase of Bi₂O₂Se thin films with high electronic performance, *Nano Res.* **16**, 3224 (2022).